

Potential energy surface interpolation with neural networks for instanton rate calculations

April M. Cooper,¹ Philipp P. Hallmen,¹ and Johannes Kästner¹

*Institute for Theoretical Chemistry, University of Stuttgart, Pfaffenwaldring 55,
70569 Stuttgart, Germany*

Artificial neural networks are used to fit a potential energy surface. We demonstrate the benefits of using not only energies, but also their first and second derivatives as training data for the neural network. This ensures smooth and accurate Hessian surfaces, which are required for rate constant calculations using instanton theory. Our aim was a local, accurate fit rather than a global PES, because instanton theory requires information on the potential only in the close vicinity of the main tunneling path. Elongations along vibrational normal modes at the transition state are used as coordinates for the neural network. The method is applied to the hydrogen abstraction reaction from methanol, calculated on a coupled-cluster level of theory. The reaction is essential in astrochemistry to explain the deuteration of methanol in the interstellar medium.

I. INTRODUCTION

Reliable information on the potential energy surface (PES) is crucial to many different applications like molecular dynamics (MD), Monte Carlo (MC) or quantum dynamics simulations. Further, a correct description of the PES is of great importance for the calculation of reaction rate constants,¹ e.g. with the instanton method. Therefore, accurate methods to obtain information on the PES are of great interest. In principle it is possible to calculate the information on the PES needed by performing ab initio energy calculations on-the-fly during the simulation process, i.e. whenever information on the PES is needed it is calculated by electronic structure theory. However, this procedure increases the time needed for the simulation significantly as the computational demand for these electronic structure calculations, from which the energy and its derivatives are obtained, is usually very high. Therefore, this approach is often infeasible.

In order to avoid this additional computational cost during the simulation, one can precompute the PES by an interpolation of ab-initio data and then use the information on the PES during the desired simulation application. Several approaches have been used to precompute PESs like spline interpolation,²⁻⁵ modified Shepard interpolation^{6,7} or interpolating moving least squares.⁸⁻¹¹ Another very promising approach is the interpolation of ab initio data with the help of artificial neural networks (NNs) to determine potential energy surfaces. This approach has become popular during the last two decades.¹²⁻³⁹

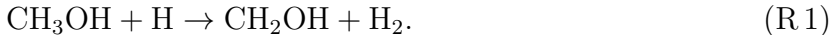
The interpolation of ab initio data with a NN allows to precompute the PES in a very accurate manner, with the result that during the actual simulation practically no computational effort is needed to request any information on the PES. Neural networks are well-suited for this task because they do not restrict the interpolation of the PES to a specific functional form. It was formally proven that artificial neural networks are universal approximators.^{28,40,41}

At present it is common practice to use only the energy during the training process of the NN. However, it was suggested in several publications^{27,35,42-44} to add information on the gradient of the energy with respect to the input coordinates. To our knowledge the use of Hessian information in the NN fit of a PES has only been reported rarely yet. In the field of minimum energy path (MEP) searches,⁴⁵⁻⁴⁸ it was shown that including Hessian information could lower the number of iterations needed to obtain a reliable MEP employing Gaussian

process regression.⁴⁸ This approach of including the gradient and Hessian information in the NN fit improves the quality of forces that are obtained from the interpolated surface because it ensures that not only the energy itself but also its gradient and Hessian are accurately fitted. For the calculation of reaction rate constants with instanton theory it is important to ensure that the energy, as well as the elements of the gradient and especially the Hessian are smooth functions of the input coordinates. Unfortunately, standard methods, like standard Shepard interpolation,⁷ often lead to spikes in the hyper surfaces describing the Hessian matrix elements and are, thus, not well-suited for the calculation of reaction rate constants with instanton theory. However, more recent variants of Shepard interpolation reduce these issues.^{49–52} Since NNs are universal approximators for smooth functions, the Hessian matrix elements can be fitted such that the resulting hyper surfaces describing the change of these with respect to the input coordinates are smooth. Therefore, we suggest an approximation of the PES by fitting a NN to information on the potential energy, gradients and Hessians in an explicit manner.

Incorporating gradient and Hessian information in the NN training increases the computational effort for the generation of each control point of the training and test sets. Nevertheless, this computational effort is feasible for the calculations of reaction rate constants where a fit to only a local part of the PES is necessary, in contrast to the global fits required for MD or MC simulations. For the calculation of rate constants with instanton theory it is sufficient to fit a comparatively small sector of the PES in the proximity of the first order saddle point that corresponds to the transition state of the reaction of interest. Further, it should be ensured that the proximity of the reactant state minimum is well described. Since the PES has to be described only locally, it is sufficient to choose comparatively few molecular configurations for the construction of the training and test set. This implies that a manageable number of ab initio calculations need to be done to allow for a good fit of the PES, which keeps the overall computational effort within reasonable bounds.

The method is applied to calculate rate constants for hydrogen abstraction from methanol by an incoming hydrogen atom,



This reaction is crucial in astrochemistry to explain the high degree of deuteration of methanol in dense clouds in the interstellar medium.⁵³

This paper is organized as follows. We give a brief overview of instanton theory to clarify why a small sector of the potential energy surface is sufficient to calculate rate constants, but why accurate Hessian information in that sector is required. Next, we describe details of the NN setup and how we use energy, gradient, and Hessian information to train the network. Then we explain how we sample the configurational space to define the control points for the training data. Next, the averaging process of independently trained NNs and the resulting error measure are described. In Results and Discussion we apply the theory to reaction (R1) and calculate rate constants with different settings.

II. METHODS

A. Instanton calculations

Semiclassical instanton theory⁵⁴⁻⁷¹ provides a way to calculate rate constants including atom tunneling based solely on geometry optimizations, i.e. without dynamical sampling. Thus, the computational effort is kept at bay. The rate constant is obtained as the imaginary part of the (logarithm of the) partition function. The latter is calculated in Feynman path integral formulation⁷² using the steepest descent approximation of the phase space integral.⁷³ In that way, the most likely tunneling path at a given temperature, the instanton, has to be located. The partition function is then calculated by taking fluctuations around the instanton path into account to quadratic order. The traditional way to find an instanton was to locate a periodic orbit on the inverted potential energy surface.⁷⁴ It is much more efficient, however, to discretize the Feynman path and search a first-order saddle point in the space of discretized Feynman paths.^{67,75} A quadratically converging search algorithm⁶⁸ allows to locate instantons efficiently in high-dimensional systems.

To calculate the rate constant k_{inst} , fluctuations around the instanton path are taken into account, leading to⁶⁸

$$k_{\text{inst}} = \sqrt{\frac{S_0}{2\pi\hbar}} \sqrt{\frac{P}{\beta\hbar}} \frac{\prod_{l=N_0+1}^{NP} \sqrt{\lambda_l^{\text{RS}}}}{\prod_{l=N_0+2}^{NP} \sqrt{|\lambda_l^{\text{inst}}|}} \exp(-S_E/\hbar) \quad (1)$$

Here, N is the number of degrees of freedom, N_0 is the number of translational and rotational degrees of freedom, P is the number of discretization points of the Feynman path (images), β is the inverse temperature, $\beta = 1/k_B T$, \hbar is Planck's constant, S_E is the Euclidean action of

the instanton path and S_0 its shortened action.⁶⁷ The values λ_l^{inst} and λ_l^{RS} are the eigenvalues of the second derivative matrix of the Euclidean action of the instanton and the reactant state, respectively, with respect to all coordinates of all images:

$$\frac{\partial^2 S_E}{\partial y_k^a \partial y_l^b} = \frac{P}{\beta \hbar} \delta_{a,b} (2\delta_{k,l} - \delta_{k-1,l} - \delta_{k,l-1}) + \frac{\beta \hbar}{P} \delta_{k,l} \frac{\partial^2 E}{\partial y_k^a \partial y_k^b} \quad (2)$$

where y_k^a is the mass-weighted coordinate component a of image k . Consequently, $\frac{\partial^2 E}{\partial y_k^a \partial y_k^b} = \nabla_k \nabla_k E$ is the second derivative (Hessian) of the potential energy of image k . Thus, Hessians of all images along the instanton path are required to calculate rate constants. The evaluation of those by on-the-fly calculations is typically the most time-consuming step during an instanton calculation. Smooth and accurate Hessians are a pre-requisite for reliable rate calculations on fitted potential energy surfaces. This is why we use them to train our NN-PES.

Translation and rotation can be taken into account separately in k_{inst} by assuming them to be decoupled from the vibrations treated in equation (1).

In this paper the Feynman paths were discretized to $P = 200$ images and the instantons were optimized such that the gradient of S_E with respect to the mass-weighted coordinates was smaller than $5.0 \cdot 10^{-11}$ atomic units. Such a small threshold is generally only achievable for PESs and derivatives with negligible numerical noise.

B. Neural Network Setup

In order to obtain a correct description of the local PES needed for the determination of the reaction rate constant, a NN is trained to predict the potential energy E that corresponds to a given configuration defined by the input coordinates x_i , $i = 1, \dots, I$. For this purpose we use a feed-forward neural network with 2 hidden layers and a single output node for the potential energy. Thereby the nodes in layer l are connected to every node in layer $l + 1$. The output of the two hidden layers y_j^1, y_k^2 and the potential energy $E = y$ were calculated

as follows:

$$y_j^1 = f^1 \left(b_j^1 + \sum_{i=1}^I (w_{j,i}^1 \cdot x_i) \right), \quad j = 1, \dots, J \quad (3)$$

$$y_k^2 = f^2 \left(b_k^2 + \sum_{j=1}^J (w_{k,j}^2 \cdot y_j^1) \right), \quad k = 1, \dots, K \quad (4)$$

$$E = y_{\text{NN}} = f^3 \left(b_1^3 + \sum_{k=1}^K (w_{1,k}^3 \cdot y_k^2) \right) \quad (5)$$

where I is the number of nodes in the input layer (number of input coordinates) and J, K are the number of nodes in the first (J) and second (K) hidden layer. Further is $w_{b,a}^l$ the weight connecting node a in layer l with node b in layer $l + 1$. Whereas b_a^l is the bias acting on node a in layer l . The transfer functions are denoted f^l , $l \in \{1, 2, 3\}$.

The transfer functions f^1 and f^2 are chosen as $f^1(\cdot) = f^2(\cdot) = \tanh(\cdot)$; f^3 is chosen to be $f^3(x) = x$ in order to allow for the prediction of arbitrary potential energy values.

In order to be able to fit not only the energy, but also the gradient and Hessian with respect to the input coordinates by a NN, these two quantities are calculated from the potential energy predicted by the NN. Thereby all emerging derivatives are calculated analytically during a backward pass through the NN by applying the chain rule. This is done to ensure that the gradient and Hessian are the analytic derivatives for a given NN PES. In principle it would also be possible to include the gradient or Hessian in the output of the NN. If these quantities would also be fitted directly by the NN, the resulting gradient and Hessian would contain small fitting errors. This, however, implies, that they are not given by the exact analytical derivatives of the potential energy and thus wouldn't be completely consistent with the energy hypersurface. Further, it is better to calculate the gradient and Hessian analytically from the energy predicted by a NN in order to keep the computational effort of the NN training at bay. Including those quantities in the NN output would require a significantly more complex structure of the NN in order to allow for sufficient flexibility for the fit. Unfortunately the computational demand of the NN training increases strongly with the number of parameters that need to be optimized during the training, i.e. the number of weights and biases. Thus, we calculate $\mathbf{g}_{\text{NN}} = \nabla E$ and $\mathbf{H}_{\text{NN}} = \nabla \nabla E$ analytically. The corresponding equations are provided in the Supporting Material.

In order to measure the quality of a NN fit a cost function has to be introduced. Commonly the mean square error of the potential energy predicted by the NN is used as a cost

function for NN fits of PESs. As not only energies, but also gradients and Hessians are to be fitted by the presented procedure, this idea of taking the mean square error of the quantities that the NN is fitted to is extended to the elements of the gradient and Hessian. Thus, the cost function R used in the training process is:

$$R = \frac{1}{N_E + N_G + N_H} \left[A_E \sum_{e=1}^{N_E} (y_{\text{NN},e} - E_{\text{ref},e})^2 + A_g \sum_{g=1}^{N_G} |\mathbf{g}_{\text{NN},g} - \mathbf{g}_{\text{ref},g}|^2 + A_H \sum_{h=1}^{N_H} |\mathbf{H}_{\text{NN},h} - \mathbf{H}_{\text{ref},h}|^2 \right]. \quad (6)$$

Thereby $|\mathbf{g}_{\text{NN},g} - \mathbf{g}_{\text{ref},g}|^2$ and $|\mathbf{H}_{\text{NN},h} - \mathbf{H}_{\text{ref},h}|^2$ are to be understood element wise, e.g.

$$|\mathbf{H}_{\text{NN},h} - \mathbf{H}_{\text{ref},h}|^2 \hat{=} \sum_{m,n=1}^I |(\mathbf{H}_{\text{NN},h})_{mn} - (\mathbf{H}_{\text{ref},h})_{mn}|^2 \quad (7)$$

The weighting parameters A_E , A_g and A_H quantify the relative influence of the errors in the energy, gradients and Hessians on the residual R . This introduces a measure of relative importance by penalizing errors in certain quantities more than in others.

During the NN training derivatives of the cost function with respect to the weights and biases need to be calculated, i.e. expressions for $\partial E/\partial w_{b,a}^l$, $\partial E/\partial b_a^l$ but also for $\partial \mathbf{g}/\partial w_{b,a}^l$, $\partial \mathbf{g}/\partial b_a^l$ and $\partial \mathbf{H}/\partial w_{b,a}^l$, $\partial \mathbf{H}/\partial b_a^l$ are required, which are tedious but straight forward to derive. These derivatives are calculated analytically in our code to ensure a proper optimization of the weights and biases. The specific expressions are provided in the Supporting Material. The cost function R is minimized using an L-BFGS algorithm.⁷⁶

Further, it can be utilized that the NN output, i.e. the potential energy, as well as the corresponding gradient and Hessian are linear in the bias and weights of the third layer, i.e. b_1^3 and $w_{1,k}^3$. Therefore, it is possible to first do a linear optimization of $w_{1,k}^3$, b_1^3 and subsequently, given these weights and biases of the third layer, optimize the remaining weights and biases with a non-linear optimization method, like the L-BFGS algorithm. This was done in the calculations presented in this paper in order to accelerate the training process.

The quality of the NN output depends strongly on the coordinate definition of the input values. Therefore, Cartesian coordinates are not well-suited as input for the NN as the NN output would change if the whole system would be translated or rotated as the system's

coordinates change. Thus, it is important to choose a coordinate description that is invariant with respect to rotations and translations. This is the reason why PESs are often fitted by NNs using internal coordinates. Since the neural network allows for a description of the input that contains redundant information it is even possible to use the set of all interatomic distances to describe the input structures.³² It is also possible to include further symmetry of the system like the interchangeability of atoms of the same species or geometrical symmetry of the structures.^{77,78} We use mass-weighted elongations along normal modes to describe the geometry of the NN input structures as these are invariant with respect to translation and rotation of the whole structure and describe the geometry uniquely. To transform from Cartesian coordinates to a normal mode description, first, the structure is superimposed with the transition state structure, which is used as the reference structure, to eliminate any relative rotations and translations of these two structures. After that the elongations of the structure with respect to the transition state structure are described by an expansion in normal modes.

To test our approach for the calculation of the reaction rate constant we fitted a PES in the proximity of the reaction path of the reaction $\text{CH}_3\text{OH} + \text{H} \rightarrow \text{CH}_2\text{OH} + \text{H}_2$ by a NN. Using the resulting PES for the energy as well as the gradient and Hessian matrix elements, we calculate the reaction rate constants for this reaction with the instanton method.

Thereby NNs with the structure 15-50-50-1 are used, i.e. there are 15 input nodes, 50 nodes in each hidden layer and one output node. The weights and biases are initialized with uniformly distributed random numbers in the interval $[-0.5, 0.5]$, b_1^3 is initialized as the average of the energies that correspond to the training set structures. The NN training is done over 5000 epochs after which we found R to be sufficiently converged. The weight factors in the cost function R are, after a preliminary parameter study, chosen to be $A_E = 1.0$, $A_g = 0.1$, $A_H = 5.0$. All parameters are given in atomic units.

C. Generation of the training and test data

The purpose of the NN training is to define a local NN PES that can be used for the calculation of reaction rate constants of one specific reaction. Therefore, the molecular structures for which the energies, gradients and Hessians were included in the training and test set were chosen along instantons at different temperatures. The chosen target level of theory

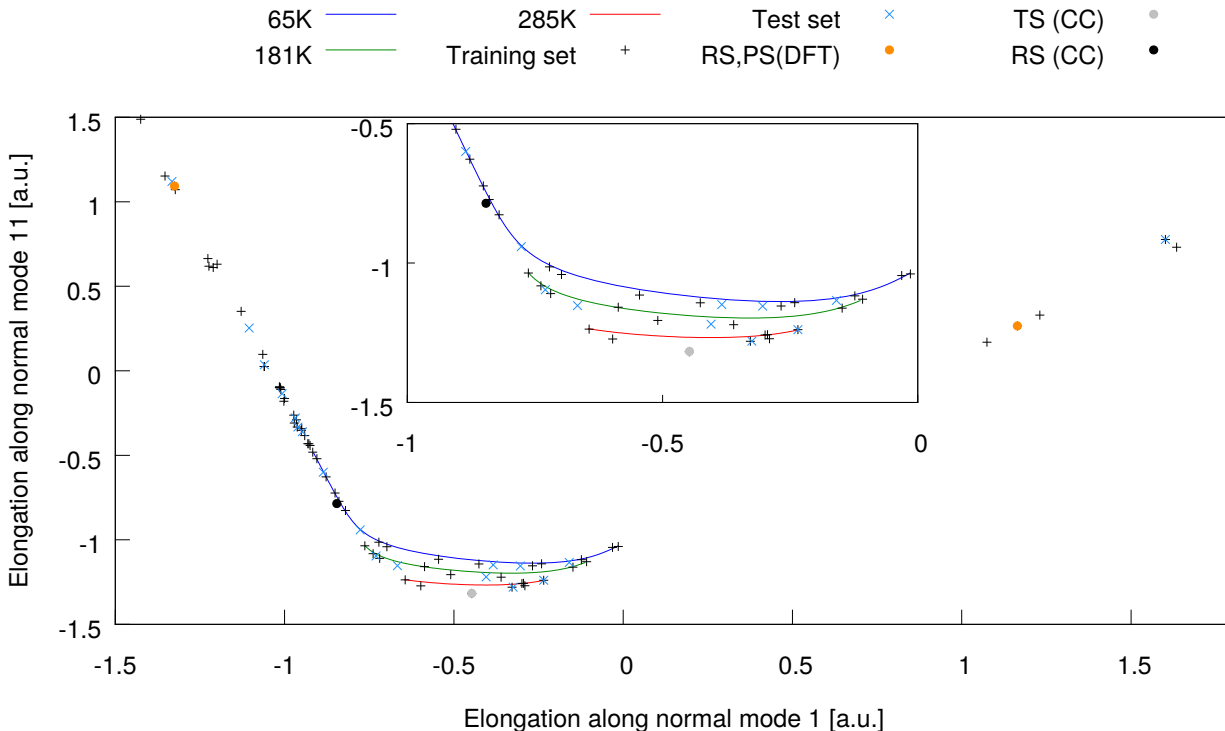


FIG. 1. Instanton paths (lines) and structures used in the NNPEs fitting process. Coordinates are given by elongations along normal modes 1 and 11. Stationary points on the different levels of theory are indicated by filled circles.

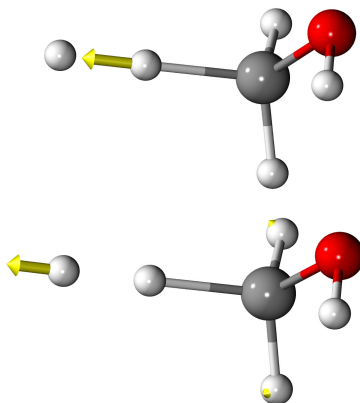


FIG. 2. Normal modes 1 and 11, on which the geometries are projected to result in Fig. 1.

is unrestricted explicitly correlated coupled-cluster theory including single and double excitations and triple-excitations approximated perturbatively, UCCSD(T)-F12/VTZ-F12, on a restricted Hartree–Fock (RHF) basis.^{79–81} Gradients and Hessians were obtained by finite

differences of energies. However, calculations of instantons on UCCSD(T)-F12/VTZ-F12 level, that require on-the-fly energy calculations, are computationally barely feasible for the reaction at hand. Thus, geometries along two instanton paths that were calculated with density functional theory on BB1K/6-311+G** level of theory⁸² at 285K and 200K were used as a starting point. This level of theory was chosen because the required computational demand is manageable and was previously⁵³ found to result in a classical transition state structure close to the one obtained from UCCSD(T) calculations extrapolated to the complete basis set. Since the region of the PES that is close to the transition state is predominantly influencing the reaction rate, a correct description of the classical transition state and its direct surroundings on the PES is crucial. The DFT calculations were performed in ChemShell^{83,84} using NWchem.⁸⁵

The training and test set were created iteratively. Initially from each of the two DFT instanton paths 20 geometries were chosen. Thereby the structures obtained from the instanton path at 285K were used as an initial training set, the others as an initial test set. Further, the geometries of the pre-reactive van-der-Waals minimum and the classical transition state were added to the training set. For every chosen geometry an ab initio calculation of the energy, the gradient and the Hessian matrix with respect to the spatial coordinates was performed on UCCSD(T)-F12/VTZ-F12 level of theory using Molpro 2012.1⁸⁶ via ChemShell^{83,84} to generate the training and test set. The initial training set contained 22 geometries, which corresponds to a total $2992 = 22 \times (1 + 15 + (15 \times 16)/2)$ unique data points, as the system was described with 15 normal modes and the Hessian is symmetric.

Using the initial setup several NNs were fitted starting from different initial weights and biases. Then instanton path optimizations were performed on the NN PESs for a large range of temperatures (285K–30K). Since the instanton path elongates with decreasing temperature and two comparatively high temperature instantons were chosen to define the initial training and test set structures, it was necessary to add further information to the training and test sets to ensure that the section of the NN PESs can describe tunneling correctly over a larger temperature range. Therefore, further structures were chosen along the instantons for temperatures in the medium to lower regime of the temperature range and their energies, gradients and Hessians were added to the training and test set.

Using this improved training and test set a new set of NNs was trained. By iterating

the interpolation of NNPEs and adding training structures for regions that are not well described yet by the NNPEs to the training set, improved training and test sets were obtained. The immediate vicinity of the pre-reactive complex is not sufficiently well described by structures chosen along instantons. However, this region must be described very precisely in order to predict reliable unimolecular reaction rate constants. Therefore, energy minimizations starting from the end point of an instanton at the side of the reactant state van-der-Waals minimum were performed. Additional structures along those minimization paths were used for the training and test set. This information improves the description of the pre-reactive complex’s vicinity by the NNPEs.

Our final training set consists of 66 reference structures, which equals to 8976 unique data points. The test set, which is defined by 18 reference structures, contains 2448 data points. The final choice of training and test set structures is shown in Fig. 1 together with instantons at three different temperatures that were calculated on a NNPE that was fitted using the final training and test set. To facilitate the visualization of the structures in Fig. 1 only their projection on the normal modes 1 and 11 are shown. These modes correspond to the movement of H_2 , see Fig. 2. The NN, however, is trained to predict the PES in the complete 15 dimensional space spanned by all normal modes. The comparatively low number of reference structures that are needed to fit the NNPE describing the reaction at hand is due to the facts that firstly only a local PES is to be fitted and secondly that the information given by the gradients and Hessians allows for a coarser sampling of the PES as they contain information on how the PES will change in the vicinity of the training and test set points.

Thus, in order to find the geometries of the training and test sets, DFT-optimizations of instantons were required to obtain an initial set of reference geometries. All other geometries were obtained by minimizations or from instanton paths calculated on NNPEs. For all these geometries energies, gradients and Hessians were calculated on the UCCSD(T)-level to train and test the NN. This approach is very efficient in CPU time requirements and extendable to larger and more complex reactions.

D. Average NN PES

In principle every NN fit will lead to a slightly different description of the PES. This is due to the fact that firstly the initial weights are chosen randomly and secondly the training is done by a local optimization of the weights and biases which can cause the training to converge to different local minima of the residual depending on the starting values of the weights and biases. However, if several NN PESs are available it is a-priori not obvious which PES is the best approximation of the physically correct PES. The final values of the cost function R are often very similar for multiple, slightly different NN PESs.

The fact that multiple NN PESs will in general differ slightly in shape also implies that reaction rate constants that are obtained on these surfaces will differ. To obtain a best estimate for the PES and a measure of its local reliability, we averaged several (N) NN PESs and used their mean to calculate instantons. Energies, gradients and Hessians were averaged. Their standard error in the energy is used to estimate the reliability of the averaged NN PES for a particular geometry. The standard error $s_{\bar{E}}$ is defined as

$$s_{\bar{E}}(\mathbf{x}) = \sqrt{\frac{\sum_{n=1}^N (E_{\text{NN},n}(\mathbf{x}) - \bar{E}_{\text{NN}}(\mathbf{x}))^2}{N(N-1)}}. \quad (8)$$

For a given input structure \mathbf{x} , $E_{\text{NN},n}$ denotes the energy of the n th individual NN and \bar{E}_{NN} is the arithmetic average of the N energies predicted for this structure. This might also reduce the influence of some local errors that might be contained in a NN PES that otherwise is a good approximation of the PESs because these small local errors can be averaged out if the other NN PESs predict a different course of the PES in these regions. Thus, the averaging serves as a way to regularize the PES and to provide an error estimate. If regions with particularly large $s_{\bar{E}}$ are reached in the instanton optimizations, additional training points have to be added.

III. RESULTS AND DISCUSSION

As an example and to demonstrate the use of NNs including gradient and Hessian information to calculate rate constants, bimolecular reaction rate constants on an average NN PES were calculated for reaction (R1).

In Fig. 3 the average potential energy along the instanton at 65 K is shown together

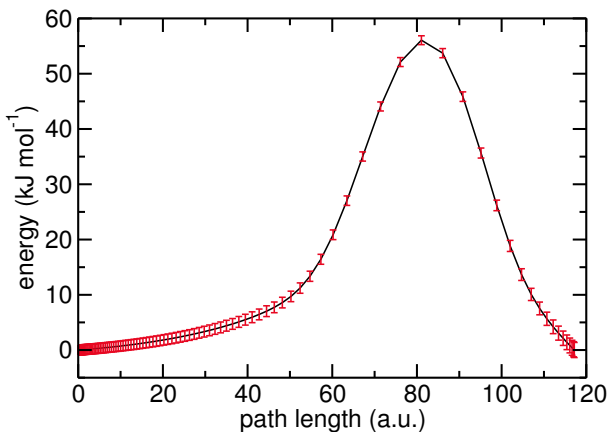


FIG. 3. Average potential energy (black) \pm 20 standard errors (red) along an instanton at $T = 65$ K. The energy is given relative to the energy of the first image.

with its corresponding standard error. The latter was multiplied by 20 to better visualize differences in the standard errors. First it has to be stated that the standard error of the average energy is very small along the whole tunneling path. The maximum standard error is about $0.027 \text{ kJ mol}^{-1}$, which indicates that the description of the energy along the reaction path is similar for all NNPEs.

In the vicinity of the transition state structure the standard error is the smallest (0.02 kJ mol^{-1}) and it increases towards the right end of the reaction path, i.e., the product state. This is due to the fact that there are fewer training points in the vicinity of the product state. Thus, there will be a greater variety between individual NNPEs in this region. However, reliable rate calculations are still possible since the error is very small even in these regions of the PES.

The small error bars of the energy along the whole tunneling path show that the energies that are predicted by the individual NNs at a certain point along the tunneling path are very similar. Therefore, taking an average of these potential surfaces should lead to a regularization of the resulting NNPEs. Consequently, performing instanton optimizations on the average surface should yield more reliable rate constants than the individual NNPEs.

All considerations made so far only covered the potential energy but not its gradient or Hessian, however. In principle it would be possible that the gradient and especially the Hessian at a specific point might deviate more from the corresponding average than the energy. We decided to test this on the rate constants themselves, rather than using the

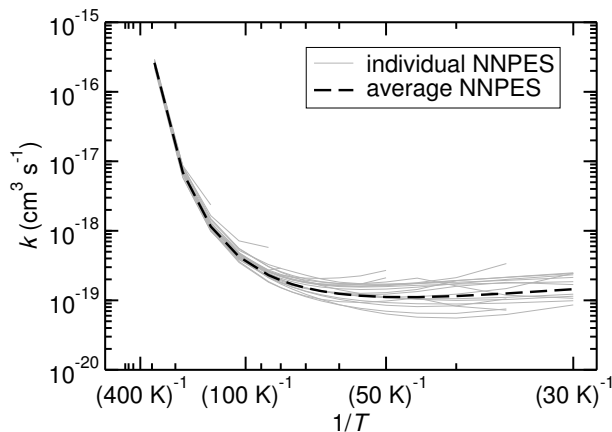


FIG. 4. Comparison of bimolecular rate constants for single NNPEs (grey) and the rate constant obtained on the average NNPE (dashed, black).

standard error of gradient or Hessian components. Therefore, we studied how strongly the rate constant for a given temperature depends on the choice of NNs which contribute to the average NNPE. Rate constants calculated on individual NNPEs, as well as on the average surface, are given in Fig. 4. At low temperature, the individual NNPEs lead to deviations in the rate constants of about a factor of 5 and somewhat uneven temperature-dependences in some cases. The average PES results in a smooth curve.

We compared results for the following three specific selections of NNPEs:

Set 1: All NNPEs for which at least one instanton optimization converged (103 NNPEs).

Set 2: All NNPEs for which the instanton optimization converged for all temperatures tested (63 NNPEs).

Set 3: All NNPEs for which the instanton optimization converged for all temperatures tested and for which a product state geometry could be found (33 NNPEs).

The average over the largest set (1) was chosen to serve as a point of reference because no pre selection of individual NNPEs has to be done. The second selection of NNPEs ensures that only those hypersurfaces enter the average which describe the shape of the barrier and the vicinity of the pre-reactive complex minimum well as otherwise the instanton optimization would not converge for all temperatures. The selection of the third set of NNPEs ensures this property as well, but it further ensures that the vicinity of the product state is described by the NNPEs with sufficient accuracy. In sets 1 and 2, there were

several NNPEs for which the product channel lead to a deep energy valley rather than a shallow vdW-minimum, which impeded convergence of the product state within the area of configuration space for which the NNPE is reliable. For these three selections of NNPEs we found very similar rate constants for the whole temperature range, see table I.

TABLE I. Reaction rate constants for different representations of the PES and deviations from the CC reference. All values at $T = 65$ K and with 60 images.

Representation of the PES	Rate constant [10^{-19} cm ³ /s]	Deviation from the CC reference[%]
CC reference	2.00	—
NNPE set 1	2.03	1.50
NNPE set 2	1.95	-2.50
NNPE set 3	2.11	5.50

As comparison, we computed one instanton directly with UCCSD(T)-F12/VTZ-F12 on-the-fly. Because of the substantial computational effort involved, we had to restrict the discretization of the instanton to 60 images. For comparison, we restricted the NNPE instanton calculation at that temperature to 60 images as well. The results are given in table I. These rate constants are all very similar. This demonstrates that the NNPE provides very accurate rate constants compared to on-the-fly calculations. The error from the fit is restricted to a few percent. The requirement in computational time is hugely reduced, though, by about 5 orders of magnitude assuming the the NN fit is already available. Overall, 74 Hessians were calculated to fit the NNPE (66 for the training set, 18 for the test set). This is comparable to the computational requirements of the on-the-fly calculation of one instanton rate constant at a single temperature (60 images, 20 optimization steps of the instanton), which required 30 Hessian calculations plus $20 \times 30 = 600$ gradient calculations. Once the NNPE is fitted, more images can be used (here: 200) and instantons at more than one temperature and with different isotopologues can be calculated with vanishing additional cost. The comparison between the NNPE-data also shows that the results within the different sets of NNPE to be averaged are very similar. Thus, the largest set 1 will be used in the following. All the errors reported here are much smaller than the expected intrinsic error of the semiclassical approximation in instanton theory or the error

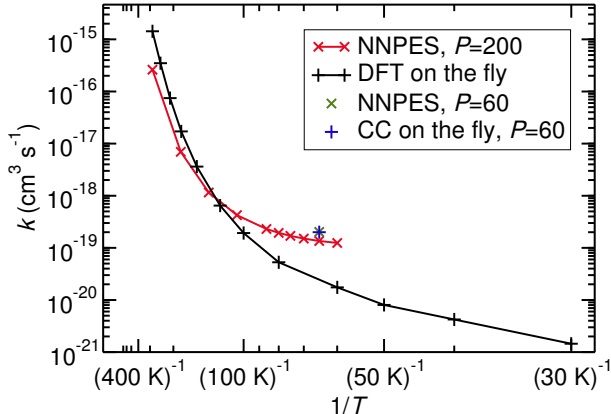


FIG. 5. Bimolecular rate constants for an average NN PES fitted on CC level (red) and from on-the-fly calculations on DFT level⁵³ (black). Reference rate constant obtained from on-the-fly calculations on CC level (blue plus sign) and reaction rate constant for the average NN PES (green cross).

caused by remaining inaccuracies of the UCCSD(T) approach.

The temperature-dependence of the rate constants that were obtained on the average NN PES with 200 images are shown in Fig. 5. The comparison clearly shows qualitative differences to the rate constants on DFT level obtained previously in our group.⁵³ The difference, up to one order of magnitude is caused by the differences in the potential between DFT and coupled cluster. The data using NN PES end at 60 K. Below that temperature, canonical instanton theory becomes inaccurate, because the tunneling energy, the energy of the turning points of the instanton, drops below the energy of the separated species. This can lead to erroneously increasing rate constants at low temperature. Microcanonical instanton theory could be used to extend the temperature range.⁸⁷ The pre-reactive vdW-minimum is less deep on the DFT-PES, which allows to calculate rate constants at even lower temperatures.

IV. CONCLUSIONS

We have shown that incorporating information on the potential energy, its gradient and Hessian in the NN training yields a NN PES with high accuracy, using relatively few training points. Averaging several NNs trained on the same data further improves the accuracy and yields a measure for the local reliability of the PES fit. The PES is especially suited for rate

calculations with instanton theory because it provides smooth and accurate second derivatives. A comparison with on-the-fly calculations of the instanton rate constant demonstrated excellent agreement. This shows that the required CPU time of calculating rate constants can be hugely reduced, by about 5 orders of magnitude, with negligible loss in accuracy.

SUPPORTING INFORMATION

Equations for additional derivatives are provided in the supporting material.

ACKNOWLEDGMENTS

This work was financially supported by the European Union’s Horizon 2020 research and innovation programme (grant agreement No. 646717, TUNNELCHEM) and the German Research Foundation (DFG) via the grant SFB 716/C.6. Computational resources were provided by the state of Baden-Württemberg through bwHPC and the German Research Foundation (DFG) through grant no INST 40/467-1 FUGG.

REFERENCES

- ¹J. Meisner and J. Kästner, *Angew. Chem. Int. Ed.* **55**, 5400 (2016).
- ²S. Chapman, M. Dupuis, and S. Green, *Chem. Phys.* **78**, 93 (1983).
- ³D. Reidel, *Approximation Theory and Spline Functions*, edited by S. Singh, J. Burry, and B. Watson, Nato Science Series C: (Springer Netherlands, Dordrecht, 2011).
- ⁴J. M. Bowman, J. S. Bittman, and L. B. Harding, *J. Chem. Phys.* **85**, 911 (1986).
- ⁵W. H. Press, S. A. Teukolsky, W. T. Vetterling, and B. P. Flannery, *Numerical Recipes: The Art of Scientific Computing*, 3rd ed. (Cambridge University Press, Cambridge, 2007).
- ⁶P. Lancaster and K. Salkauskas, *Curve and surface fitting: an introduction*, 3rd ed. (Academic Press, New York, 1986).
- ⁷R. Farwig, J. Mason, and M. Cox, “Algorithms for approximation,” (1987).
- ⁸T. Ishida and G. C. Schatz, *Chem. Phys. Lett.* **314**, 369 (1999).
- ⁹G. G. Maisuradze, D. L. Thompson, A. F. Wagner, and M. Minkoff, *J. Chem. Phys.* **119**, 10002 (2003).

- ¹⁰Y. Guo, A. Kawano, D. L. Thompson, A. F. Wagner, and M. Minkoff, *J. Chem. Phys.* **121**, 5091 (2004).
- ¹¹R. Dawes, D. L. Thompson, Y. Guo, A. F. Wagner, and M. Minkoff, *J. Chem. Phys.* **126**, 184108 (2007).
- ¹²T. Blank and S. Brown, *Anal. Chim. Acta.* **277**, 273 (1993).
- ¹³J. Gasteiger and J. Zupan, *Angew. Chem. Int. Ed.* **32**, 503 (1993).
- ¹⁴T. B. Blank, S. D. Brown, A. W. Calhoun, and D. J. Doren, *J. Chem. Phys.* **103**, 4129 (1995).
- ¹⁵E. Tafeit, W. Estelberger, R. Horejsi, R. Moeller, K. Oettl, K. Vrecko, and G. Reibnegger, *J. Mol. Graph.* **14**, 12 (1996).
- ¹⁶D. F. R. Brown, M. N. Gibbs, and D. C. Clary, *J. Chem. Phys.* **105**, 7597 (1996).
- ¹⁷K. T. No, B. H. Chang, S. Y. Kim, M. S. Jhon, and H. A. Scheraga, *Chem. Phys. Lett.* **271**, 152 (1997).
- ¹⁸H. Gassner, M. Probst, A. Lauenstein, and K. Hermansson, *J. Phys. Chem. A* **102**, 4596 (1998).
- ¹⁹F. V. Prudente and J. J. S. Neto, *Chem. Phys. Lett.* **287**, 585 (1998).
- ²⁰F. V. Prudente, P. H. Acioli, and J. J. S. Neto, *J. Chem. Phys.* **109**, 8801 (1998).
- ²¹C. Muoz-Caro and A. Nio, *Comput. Chem.* **22**, 355 (1998).
- ²²S. Hobday, R. Smith, and J. BelBruno, *Nucl. Instrum. Methods Phys. Res. B* **153**, 247 (1999).
- ²³K.-H. Cho, K. T. No, and H. A. Scheraga, *J. Mol. Struct.* **641**, 77 (2002).
- ²⁴T. M. Rocha Filho, Z. T. Oliveira Jr., L. A. C. Malbouisson, R. Gargano, and J. J. Soares Neto, *Int. J. Quantum Chem.* **95**, 281 (2003).
- ²⁵A. C. P. Bittencourt, F. V. Prudente, and J. D. M. Vianna, *Chem. Phys.* **297**, 153 (2004).
- ²⁶S. Lorenz, A. Groß, and M. Scheffler, *Chem. Phys. Lett.* **395**, 210 (2004).
- ²⁷J. B. Witkoskie and D. J. Doren, *J. Chem. Theory Comput.* **1**, 14 (2005).
- ²⁸S. Manzhos, X. Wang, R. Dawes, and T. Carrington, *J. Phys. Chem. A* **110**, 5295 (2006).
- ²⁹S. Manzhos and T. Carrington Jr., *J. Chem. Phys.* **125**, 084109 (2006).
- ³⁰S. Manzhos and T. Carrington Jr., *J. Chem. Phys.* **125**, 194105 (2006).
- ³¹P. M. Agrawal, L. M. Raff, M. T. Hagan, and R. Komanduri, *J. Chem. Phys.* **124**, 134306 (2006).

- ³²D. I. Doughan, L. M. Raff, M. G. Rockley, M. Hagan, P. M. Agrawal, and R. Komanduri, *J. Chem. Phys.* **124**, 054321 (2006).
- ³³M. Malshe, L. M. Raff, M. G. Rockley, M. Hagan, P. M. Agrawal, and R. Komanduri, *J. Chem. Phys.* **127**, 134105 (2007).
- ³⁴H. M. Le, S. Huynh, and L. M. Raff, *J. Chem. Phys.* **131**, 014107 (2009).
- ³⁵A. Pukrittayakamee, M. Malshe, M. Hagan, L. M. Raff, R. Narulkar, S. Bukkapatnum, and R. Komanduri, *J. Chem. Phys.* **130**, 134101 (2009).
- ³⁶C. M. Handley and P. L. A. Popelier, *J. Phys. Chem. A* **114**, 3371 (2010).
- ³⁷J. Behler, in *Chemical Modelling: Applications and Theory Volume 7*, Vol. 7 (The Royal Society of Chemistry, 2010) pp. 1–41.
- ³⁸J. Chen, X. Xu, X. Xu, and D. H. Zhang, *J. Chem. Phys.* **138**, 154301 (2013).
- ³⁹J. Yuan, D. He, and M. Chen, *Phys. Chem. Chem. Phys.* **17**, 11732 (2015).
- ⁴⁰J. Ludwig and D. G. Vlachos, *J. Chem. Phys.* **127**, 154716 (2007).
- ⁴¹H. M. Le and L. M. Raff, *J. Phys. Chem. A* **114**, 45 (2010).
- ⁴²S. Ferrari and R. F. Stengel, *IEEE Trans. Neural Netw.* **16**, 24 (2005).
- ⁴³J. Behler, *Phys. Chem. Chem. Phys.* **13**, 17930 (2011).
- ⁴⁴N. Artrith, T. Morawietz, and J. Behler, *Phys. Rev. B* **83**, 153101 (2011).
- ⁴⁵A. A. Peterson, *J. Chem. Phys.* **145**, 074106 (2016).
- ⁴⁶A. Khorshidi and A. A. Peterson, *Comp. Phys. Commun.* **207**, 310 (2016).
- ⁴⁷A. A. Peterson, R. Christensen, and A. Khorshidi, *Phys. Chem. Chem. Phys.* **19**, 10978 (2017).
- ⁴⁸O.-P. Koistinen, F. B. Dagbjartsdttir, V. Ásgeirsson, A. Vehtari, and H. Jónsson, *J. Chem. Phys.* **147**, 152720 (2017).
- ⁴⁹R. P. A. Bettens and M. A. Collins, *J. Chem. Phys.* **111**, 816 (1999).
- ⁵⁰M. Yang, D. H. Zhang, M. A. Collins, and S.-Y. Lee, *J. Chem. Phys.* **115**, 174 (2001).
- ⁵¹M. A. Collins, *Theor. Chem. Acc.* **108**, 313 (2002).
- ⁵²T. J. Frankcombe, *J. Chem. Phys.* **140**, 114108 (2014).
- ⁵³T. P. M. Goumans and J. Kästner, *J. Phys. Chem. A* **115**, 10767 (2011).
- ⁵⁴J. S. Langer, *Ann. Phys. (N.Y.)* **41**, 108 (1967).
- ⁵⁵J. S. Langer, *Ann. Phys. (N.Y.)* **54**, 258 (1969).
- ⁵⁶W. Miller, *J. Chem. Phys.* **62**, 1899 (1975).
- ⁵⁷C. G. Callan Jr. and S. Coleman, *Phys. Rev. D* **16**, 1762 (1977).

- ⁵⁸E. Gildener and A. Patrascioiu, *Phys. Rev. D* **16**, 423 (1977).
- ⁵⁹I. Affleck, *Phys. Rev. Lett.* **46**, 388 (1981).
- ⁶⁰S. Coleman, *Nucl. Phys. B* **298**, 178 (1988).
- ⁶¹P. Hänggi, P. Talkner, and M. Borkovec, *Rev. Mod. Phys.* **62**, 251 (1990).
- ⁶²V. A. Benderskii, D. E. Makarov, and C. A. Wight, *Adv. Chem. Phys.* **88**, 55 (1994).
- ⁶³M. Messina, G. K. Schenter, and B. C. Garrett, *J. Chem. Phys.* **103**, 3430 (1995).
- ⁶⁴J. O. Richardson and S. C. Althorpe, *J. Chem. Phys.* **131**, 214106 (2009).
- ⁶⁵M. Kryvohuz, *J. Chem. Phys.* **134**, 114103 (2011).
- ⁶⁶S. C. Althorpe, *J. Chem. Phys.* **134**, 114104 (2011).
- ⁶⁷J. B. Rommel, T. P. M. Goumans, and J. Kästner, *J. Chem. Theory Comput.* **7**, 690 (2011).
- ⁶⁸J. B. Rommel and J. Kästner, *J. Chem. Phys.* **134**, 184107 (2011).
- ⁶⁹M. Kryvohuz, *J. Phys. Chem. A* **118**, 535 (2014).
- ⁷⁰Y. Zhang, J. B. Rommel, M. T. Cvitaš, and S. C. Althorpe, *Phys. Chem. Chem. Phys.* **16**, 24292 (2014).
- ⁷¹J. O. Richardson, *J. Chem. Phys.* **144**, 114106 (2016).
- ⁷²R. P. Feynman, *Rev. Mod. Phys.* **20**, 367 (1948).
- ⁷³J. Kästner, *WIREs Comput. Mol. Sci.* **4**, 158 (2014).
- ⁷⁴M. Ceotto, *Mol. Phys.* **110**, 547 (2012).
- ⁷⁵S. Andersson, G. Nyman, A. Arnaldsson, U. Manthe, and H. Jónsson, *J. Phys. Chem. A* **113**, 4468 (2009).
- ⁷⁶D. C. Liu and J. Nocedal, *Math. Prog.* **45**, 503 (1989).
- ⁷⁷J. Behler, *J. Chem. Phys.* **134**, 074106 (2011).
- ⁷⁸J. S. Smith, O. Isayev, and A. E. Roitberg, *Chem. Sci.* **8**, 3192 (2017).
- ⁷⁹T. B. Adler, G. Knizia, and H.-J. Werner, *J. Chem. Phys.* **127**, 221106 (2007).
- ⁸⁰K. A. Peterson, T. B. Adler, and H.-J. Werner, *J. Chem. Phys.* **128**, 084102 (2008).
- ⁸¹G. Knizia, T. B. Adler, and H.-J. Werner, *J. Chem. Phys.* **130**, 054104 (2009).
- ⁸²Y. Zhao, B. J. Lynch, and D. G. Truhlar, *J. Phys. Chem. A* **108**, 2715 (2004).
- ⁸³P. Sherwood, A. H. de Vries, M. F. Guest, G. Schreckenbach, C. R. A. Catlow, S. A. French, A. A. Sokol, S. T. Bromley, W. Thiel, A. J. Turner, S. Billeter, F. Terstegen, S. Thiel, J. Kendrick, S. C. Rogers, J. Casci, M. Watson, F. King, E. Karlsen, M. Sjøvoll, A. Fahmi, A. Schäfer, and C. Lennartz, *J. Mol. Struct. (THEOCHEM)* **632**, 1 (2003).

- ⁸⁴S. Metz, J. Kästner, A. A. Sokol, T. W. Keal, and P. Sherwood, *WIREs Comput. Mol. Sci.* **4**, 101 (2014).
- ⁸⁵M. Valiev, E. J. Bylaska, N. Govind, K. Kowalski, T. P. Straatsma, H. J. J. van Dam, D. Wang, J. Nieplocha, E. Apra, T. L. Windus, and W. A. de Jong, *Comput. Phys. Commun.* **181**, 1477 (2010).
- ⁸⁶H.-J. Werner, P. J. Knowles, G. Knizia, F. R. Manby, M. Schütz, *et al.*, “Molpro, version 2012.1, a package of ab initio programs,” (2015).
- ⁸⁷S. R. McConnell, A. Löhle, and J. Kästner, *J. Chem. Phys.* **146**, 074105 (2017).